

# Complete Wetting of Nanosculptured Substrates

M. Tasinkevych<sup>1,2</sup> and S. Dietrich<sup>1,2</sup>

<sup>1</sup>*Max-Planck-Institut für Metallforschung,*

*Heisenbergstr. 3, D-70569 Stuttgart, Germany*

<sup>2</sup>*Institut für Theoretische und Angewandte Physik,*

*Universität Stuttgart, Pfaffenwaldring 57, D-70569 Stuttgart, Germany*

(Dated: March 23, 2022)

## Abstract

Complete wetting of geometrically structured substrates by one-component fluids with long-ranged interactions is studied. We consider periodic arrays of rectangular or parabolic grooves and lattices of cylindrical or parabolic pits. We show that the midpoint interfacial heights within grooves and pits are related in the same way as for complete wedge and cone filling. For sufficiently deep cavities with vertical walls and small undersaturation, an effective planar scaling regime emerges. The scaling exponent is  $-1/3$  in all cases studied, and only the amplitudes depend on the geometrical features. We find quantitative agreement with recent experimental data for such systems.

PACS numbers: 68.08.Bc, 68.08.-p, 05.70.Np

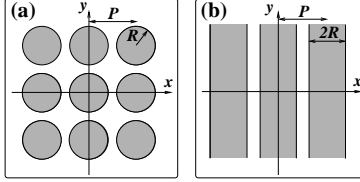


FIG. 1: Top view of the substrate geometries. (a) Quadratic lattice of identical pits (cylinders or paraboloids). (b) Periodic array of grooves (rectangular or parabolic). All cavities have finite depths  $D$ .

The growing interest in device miniaturization has led to the emergence of various experimental techniques of tailoring the geometrical and chemical topography of solid surfaces at mesoscopic scales [1, 2]. Such nano-patterning of the surfaces may result in drastic changes of their wetting characteristics, which is important for technologies such as micro-fluidics [3] or the fabrication of super-hydrophobic or super-hydrophilic surfaces [2]. Experimental studies of complete wetting on sculptured surfaces [4, 5] demonstrate the strong influence of nanocavities on the adsorption behavior relative to that of flat substrates. Theoretical studies of adsorption in infinitely deep generalized wedges [6] predict geometry dependent wetting exponents.

Although it is known that a non-planar topography of a substrate modifies its wetting by a fluid, recent studies have revealed surprising hidden symmetries, or so-called covariances, which relate various local adsorption properties for different substrate geometries. These covariances imply that different confining potentials can lead to identical local interfacial properties once external fields are suitably rescaled. For instance, for both long- and short-ranged forces, complete wetting at the apex of a wedge can be mapped onto critical wetting of a planar substrate with the apex angle playing the role of the contact angle [7], which maps one-to-one to temperature. In two-dimensional systems, critical wedge filling can be related to the strong-fluctuation regime of critical planar wetting [8]. Recently, a new example of geometrical covariance relating wedge and cone complete filling has been reported [9] showing that the equilibrium midpoint interfacial heights  $l^{(0)}$  in a cone and a wedge obey the relation  $l_c^{(0)}(\Delta\mu, \alpha) = l_w^{(0)}(\Delta\mu/2, \alpha)$  with  $\alpha$  being the substrate tilt angle and  $\Delta\mu \geq 0$  the chemical potential deviation from liquid-vapor coexistence. This relation is valid for the leading behaviors of  $l$  in the limit  $\Delta\mu \rightarrow 0^+$ .

Based on an effective interface Hamiltonian in the following we demonstrate that complete wetting of substrates patterned by periodic arrays of grooves or quadratic lattices of pits (see Fig. 1), both of depths  $D$ , exhibits a geometrical covariance similar to the one described in Ref. [9]. We consider rectangular or parabolic grooves and cylindrical or parabolic pits, taking into account the long range of the intermolecular potentials. We observe four different scaling regimes: filling, post-filling, effective planar, and planar, with the neighboring regimes being separated by, as we call,  $\Delta\mu_{fil}^{p,g} > \Delta\mu_\pi^e > \Delta\mu_\pi$ . The aforementioned covariance relates the behavior of the midpoint wetting film thicknesses for all geometries and holds within an undersaturation range  $\Delta\mu_\pi^e \lesssim \Delta\mu \lesssim \Delta\mu_{fil}^{p,g}(R)$  (for  $\Delta\mu_\pi^e$  see below, the superscripts  $p, g$  refer to *pits* and *grooves*, respectively) which we call the *post-filling scaling regime*. In the case of cylindrical pits or rectangular grooves, for  $\Delta\mu \searrow \Delta\mu_{fil}^{p,g}(R)$  and for sufficiently large  $D/R$ , the analogue of capillary condensation occurs such that the pits or grooves are rapidly, but continuously, filled by the liquid. However, in the case of the parabolically shaped pits or grooves,  $\Delta\mu_{fil}^{p,g}$  marks the crossover from the continuous power-law filling regime at  $\Delta\mu > \Delta\mu_{fil}^{p,g}$ , to the post-filling scaling regime. We find numerically for  $R/\sigma \gtrsim 50$  (see Fig. 1), where  $\sigma$  is a molecular length scale,  $\Delta\mu_{fil}^{p,g}(R) \sim R^{-1-\delta}$  with a small positive effective exponent  $\delta$ , and  $\Delta\mu_{fil}^p = 2\Delta\mu_{fil}^g$ . If we denote the equilibrium interface height at the position of the symmetry axes of the cylindrical or parabolic pits as  $l_p^{(0)}$ , and in the middle of the rectangular or parabolic grooves as  $l_g^{(0)}$ , we obtain in the post-filling regime

$$l_{p,g}^{(0)}(\Delta\mu, R, P, D) = R\Lambda_{p,g}\left((\Delta\mu/\varepsilon_f)(R/\sigma)^{1+\delta}\right),$$

$$\Lambda_p(x) = \Lambda_g(x/2). \quad (1)$$

The scaling functions  $\Lambda_{p,g}(x)$  do not depend on  $D$  and  $P$ , i.e., in this regime the midpoint interfacial heights increase upon decreasing undersaturation in the same way for an isolated cavity as for arrays of them;  $\varepsilon_f$  is a molecular energy scale.

For  $\Delta\mu < \Delta\mu_\pi^e$  the cavities are completely filled by the liquid and the equilibrium interface heights  $l_{p,g}(x, y) = l_{p,g}$  become de facto independent of the lateral coordinates  $\mathbf{x} \equiv (x, y)$ . In the case of the rectangular grooves or cylindrical pits,  $\Delta\mu_\pi^e$  marks the crossover from the post-filling scaling regime to the *effective planar scaling regime* within which the wetting behavior of geometrically patterned substrates can be mapped onto that of layered flat solids. The upper layer of those solids has a thickness  $D$ , and its composition is related to

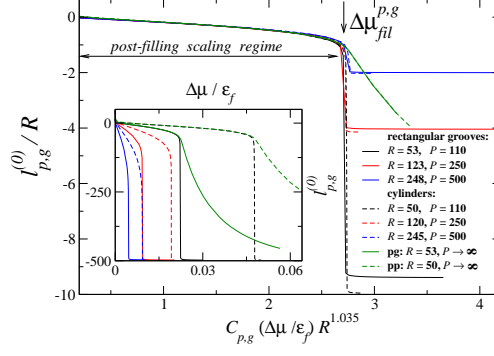


FIG. 2: Interfacial heights  $l_{p,g}^{(0)}$  (measured from the top substrate layer  $z = 0$ ) at the middle of the cylindrical and parabolic pits,  $l_p^{(0)}$  (dashed lines), and of the rectangular and parabolic grooves,  $l_g^{(0)}$  (solid lines), as a function of  $\Delta\mu$  with  $C_p = 1$  and  $C_g = 2$ . Rescaling the variables according to Eq.(1) leads to data collapse. The inset shows the same data unscaled. The depth of the cavities is  $D = 500$ ;  $pp(g)$  denotes parabolic pits (grooves). All length are measured in units of  $\sigma$ .

the geometrical parameters  $R$  and  $P$ . This results in the following scaling relations for the effective planar scaling regime:

$$l_{p,g}(\Delta\mu, R, P, D) = (\Phi_{p,g})^{\frac{1}{3}} l_{\pi}(\Delta\mu), \quad (2)$$

where  $l_{\pi}$  is the thickness of the adsorbed liquid film on the corresponding non-patterned planar substrate.  $\Phi_p = 1 - \pi(R/P)^2$  and  $\Phi_g = 1 - 2R/P$  are the areal fractions of solid in the top layer,  $z = 0$ , of substrates with cylindrical pit and rectangular groove patterns, respectively. This result is reminiscent of the Cassie equation [10] describing the apparent contact angle on chemically structured substrates. For  $D \rightarrow 0$  the width of the effective planar regime, i.e., the range of applicability of Eq. 2 vanishes.

Finally, at  $\Delta\mu = \Delta\mu_{\pi} \sim D^{-3}$  with  $\Delta\mu_{\pi} < \Delta\mu_{\pi}^e$  the systems cross over to the *planar scaling* regime, in which the geometrical patterns are irrelevant. This crossover occurs only for long-ranged dispersion forces; we consider only them throughout. (For short-ranged interactions, instead, the growth of the wetting film would remain determined by the areal fraction of solid at  $z = 0$  for all film thicknesses.) In the case of the parabolic pits and grooves, we do not observe the effective planar scaling regime. There is rather an extended crossover region from the post-filling scaling regime to the planar one.

We base our calculations on the effective interface Hamiltonian description [11]

$$H[l] = \iint d^2x \left( \sigma_{lg} \sqrt{1 + (\nabla l)^2} + \Delta\mu \Delta\rho l + W(\mathbf{x}, l) \right), \quad (3)$$

where  $l(\mathbf{x})$  denotes the local interfacial height which is measured from the plane  $z = 0$  where the substrate ends,  $\sigma_{lg}$  is the surface tension of the free liquid-vapor interface,  $\Delta\rho = \rho_l - \rho_g$  is the difference in number densities of the coexisting bulk phases, and  $W(\mathbf{x}, l)$  is the effective interface potential. The functional in Eq. (3) can be derived systematically from microscopic density functional theory, which allows one to determine the explicit functional form of  $W(\mathbf{x}, l)$  for a given substrate shape and its dependence on the fluid-fluid and substrate-fluid interaction potentials. We approximate the attractive parts of the pair potentials by  $\phi_{f,s}(r) = -\frac{128\sqrt{2}}{9\pi}\varepsilon_{f,s}\sigma^6(\sigma^2 + r^2)^{-3}$ . The amplitude is chosen such that the integrated strength of  $\phi_f$  equals that of the attractive contribution of the Lennard-Jones potential obtained by a strict application of the Weeks-Chandler-Andersen procedure. This leads to the effective interface potential

$$\begin{aligned} W_\Omega(\mathbf{x}, l) &= A \times I_\Omega(\mathbf{x}, l), \\ I_\Omega(\mathbf{x}, l) &= \int_l^\infty dz \int_\Omega d^3r' (\sigma^2 + |\mathbf{r} - \mathbf{r}'|^2)^{-3}, \end{aligned} \quad (4)$$

where  $A = -\frac{128\sqrt{2}}{9\pi}\sigma^6\Delta\rho(\rho_l\varepsilon_f - \rho_s\varepsilon_s) > 0$  is an effective Hamaker constant with  $\rho_s$  as the number density of the substrate, and  $\Omega$  denotes the domain occupied by substrate particles. The effective interface potential of the planar substrate is  $W_\pi(l \gg \sigma) \approx A\pi/(12l^2)$  so that  $l_\pi(\Delta\mu \rightarrow 0) = (A\pi/(12\Delta\rho\Delta\mu))^{1/3}$ .

In the following we minimize the functional in Eq. (3) numerically, which yields the equilibrium interface height  $l(\mathbf{x})$  within mean-field theory which is valid in  $d = 3$  for complete wetting [11] and filling [9] for the dispersion forces considered here. For all substrate geometries the midpoint heights  $l_{p,g}^{(0)}(\Delta\mu)$  exhibit four different regimes. The first regime corresponds to the filling of the cavities. For the case of rectangular grooves and cylindrical pits, and for  $D/R$  large enough, a quasi abrupt, but still continuous filling of the cavities takes place at  $\Delta\mu = \Delta\mu_{fil}^{p,g}$ , which is shown in the inset of Fig. 2. A similar behavior has been reported earlier for an isolated rectangular groove [12]. We find that the locus  $\Delta\mu_{fil}^{p,g}$  of the filling transformation scales with the lateral size of the cavities as  $R^{-1-\delta}$ , with an effective exponent  $\delta \approx 0.035$  for both the rectangular grooves and the cylindrical pits. For the case of parabolic pits and grooves, complete filling of the structures is described by an

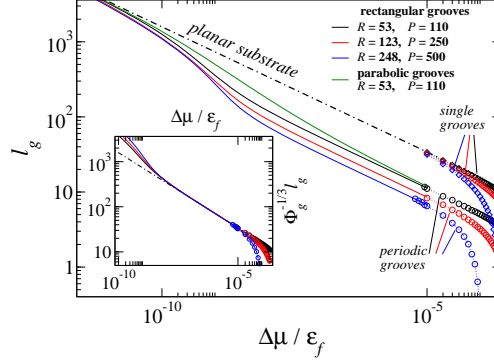


FIG. 3: Wetting film thickness  $l_g$  above grooves for small  $\Delta\mu$ . The symbols represent the midpoint interfacial height  $l_g^{(0)}$ . The solid lines are obtained by minimizing Eq.(3) assuming  $l(\mathbf{x}) = l_g$ . On the present scales they are indistinguishable from those for film thicknesses  $l_\pi^e(\Delta\mu)$  on layered and flat ersatz substrates, with a top layer of height  $D$  and an effective Hamaker constant  $A^e = A\Phi_g$ , where  $A$  is the Hamaker constant of the solid without grooves. In the inset the vertical axis is rescaled according to Eq. (2) leading to data collapse within an intermediate regime, the width of which increases as  $\Delta\mu_\pi^e - \text{const} \times D^{-3}$  for  $D \rightarrow \infty$ . The groove depth is  $D = 500$ .

effective power law,  $l_{p,g}^{(0)}(\Delta\mu, R, D) \sim \Delta\mu^{-\gamma(R,D)}$  valid for  $\Delta\mu \gtrsim \Delta\mu_{fil}^{p,g}$ . We find the values of the effective exponent  $\gamma$  ranging from ca. 3.1, for  $R = 245\sigma$ , to ca. 2.0, for  $R = 50\sigma$ , at a cavity depth  $D = 500\sigma$ . Moreover, the complete filling of the parabolic cavities obeys the covariance relation  $l_p^{(0)}(\Delta\mu, R, D) = l_g^{(0)}(\Delta\mu/2, R, D)$ .

In the second, post-filling regime, i.e., for  $\Delta\mu \in (\Delta\mu_\pi^e, \Delta\mu_{fil}^{p,g})$ , the midpoint height for all patterns shows an almost linear dependence on  $\Delta\mu$  on normal scales. The morphologies of the liquid films still reflect the geometrical patterns, i.e., there are considerable lateral variations of the interfacial heights. We find that the slopes of the  $l_{p,g}^{(0)}$  curves scale as  $R^\alpha$  with  $\alpha \approx 2$ . Thus, combining this fact with the scaling of the filling chemical potential  $\Delta\mu_{fil}^{p,g}$ , we propose for the functions  $l_{p,g}^{(0)}$  in the post-filling regime the scaling forms given by Eq. (1). The scaling functions  $\Lambda_{p,g}$  and the corresponding data collapse upon suitably rescaling the chemical potential are shown in Fig. 2. The scaling functions  $\Lambda_{p,g}$  in the post-filling regime do not depend on the cavity depth  $D$  and the pattern periodicity  $P$ . In the case of a single cavity, i.e., in the limit  $P \rightarrow \infty$ , we obtain the same curves  $l_{p,g}^{(0)}(\Delta\mu)$  as those presented in Fig. 2.

Below a certain value  $\Delta\mu_\pi^e$  the interface height becomes de facto flat, denoted as  $l_{p,g}$

for the respective patterns. In this case the functional in Eq. (3) reduces to a function of  $l_{p,g}$  the minimum of which determines the thicknesses of the wetting films in this regime. Figure 3 shows the functions  $l_g(\Delta\mu)$  for several values of  $R$  and  $P$  as well as the planar film thickness  $l_\pi(\Delta\mu)$ . The rectangular groove (and cylindrical pit, not shown) geometries lead to the same power law behavior as for a flat surface,  $l_{p,g} \sim \Delta\mu^{-1/3}$ , but with different amplitudes reflecting different effective Hamaker constants, which depend on the geometry of the patterns. We call this behavior the effective planar scaling regime.  $l_g(\Delta\mu)$  for the parabolic grooves does not reveal the effective planar scaling regime, but gradually crosses over to the planar one,  $l_\pi$ . In order to find the geometrical dependence of the amplitudes of the scaling laws given above, we mimic sculptured substrates by layered and flat ersatz solids, with the effective interface potential  $W(l \gg \sigma) \approx \frac{\pi}{12} (A^e/l^2 + (A - A^e)/(l + D)^2)$  [13]. The first term is the effective interface potential of a flat semi-infinite solid with Hamaker constant  $A^e$  and the second term is the correction due to the actual bottom part of the substrate,  $z \in (-\infty, -D)$ , with Hamaker constant  $A$ . For  $\sigma \ll l \lesssim D$ , to a good approximation one may ignore the bottom part of the substrate (i.e., the second term in  $W(l \gg \sigma)$ ) so that the amplitude is determined by the Hamaker constant  $A^e$ . Consider a lateral unit cell  $\omega_0$  of this sculptured part of the substrate ( $z \in [-D, 0]$ ), with  $\omega_s$  as its domain occupied by the solid. By requiring  $W_{\cup\omega_s}(\mathbf{x}, l) = W_{\cup\omega_0}^e(\mathbf{x}, l)$ , we obtain for the effective Hamaker constant  $A^e = AI_{\cup\omega_s}(\mathbf{x}, l)/I_{\cup\omega_0}(\mathbf{x}, l)$ , where  $W_{\cup\omega_0}^e$  is the effective interface potential generated by the laterally homogeneous top layer of the layered and flat ersatz substrate; the symbol  $\cup$  denotes the union of domains. For  $l \gg \sigma$  the integrals  $I_{\cup\omega_i}$  ( $i = s, 0$ ) can be approximated as:

$$I_{\cup\omega_i} \approx \int_l^\infty dz \int_{\cup\omega_i} \frac{d^3r'}{(z - z')^6} \left( 1 - 3 \frac{\sigma^2 + \|\mathbf{x} - \mathbf{x}'\|^2}{(z - z')^2} \right). \quad (5)$$

In Eq. (5) the leading term as function of  $l$  renders  $A^e \approx AS_s/S_0$ , where  $S_i$  is the surface area of the domain  $\omega_i \cap \{(\mathbf{x}, z = 0)\}$ . Thus, we obtain  $A_g^e \approx A\Phi_g$  for the rectangular grooves and  $A_p^e \approx A\Phi_p$  for cylindrical pits (see Eq. (2)). The thicknesses  $l_\pi^e(\Delta\mu)$  of the wetting films on such layered ersatz substrates, which effectively correspond to arrays of grooves, are almost indistinguishable from the corresponding ones for  $l_g$ . Therefore, we conclude that, for sufficiently thick wetting films,  $l_g$  obeys the scaling relation given in Eq. (2). Indeed, after rescaling by the geometry-dependent factors  $(\Phi_g)^{-1/3}$ , the curves for  $l_g$  collapse and, within the numerical precision, coincide with the curve for  $l_\pi$ . This is shown in the inset

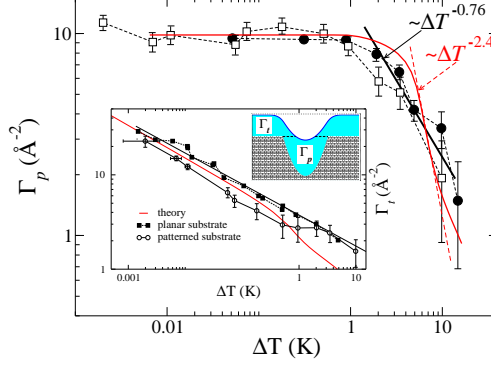


FIG. 4: Liquid adsorption at parabolic pits. Inset:  $\Gamma_t(\Delta T)$ . Red line – theory; symbols and black lines – experimental data from Ref. [4] (where  $\Gamma_p$  is denoted as  $\Gamma_c$ ).  $\Delta T$  is proportional to  $\Delta\mu$  (see main text).

of Fig. 3. In the case of a lattice of cylindrical pits we observe the same behavior of the corresponding  $l_p$  curves (not shown). As  $l_g$  reaches the value  $\sim D$ , i.e., at  $\Delta\mu = \Delta\mu_\pi \sim D^{-3}$ , a crossover to the *planar scaling regime* takes place. In the planar scaling regime  $\Delta\mu \lesssim \Delta\mu_\pi$  the geometrical patterns are irrelevant. As  $D$  decreases,  $\Delta\mu_\pi$  eventually merges with  $\Delta\mu_\pi^e$ , eliminating the effective planar scaling regime.

Figure 4 compares our results with the corresponding experimental data of Ref. [4], in which the adsorption of methylcyclohexane (MCH) on a silicon substrate sculptured by a hexagonal lattice of parabolic pits has been studied with the following geometrical parameters: depth  $D \approx 200\text{\AA}$ ; radius of the pits at the opening  $R \approx 123\text{\AA}$ ; lattice constant  $P \approx 394\text{\AA}$ . As in Ref. [4], we display the volume  $\Gamma = \Gamma_p + \Gamma_t$  of adsorbed liquid divided by the projected area and multiplied by the electron density of the bulk fluid as the sum of the amount  $\Gamma_p$  adsorbed in the pit, and the amount  $\Gamma_t$  adsorbed above the pit opening. For MCH we adopt the Lennard-Jones parameters  $\sigma = 5.511\text{\AA}$  and  $\varepsilon_f/k_B = 446\text{K}$  [14]. Then the relation between the undersaturation  $\Delta\mu$  and the reservoir-substrate temperature difference (used in the experiment as a means to tune the deviation from liquid-vapor coexistence) is  $\Delta T \approx 32.37 \frac{\Delta\mu}{\varepsilon_f} K$ . Fitting the film thickness on the planar substrate to the corresponding experimental curve fixes the value of the Hamaker constant. For the liquid-vapor surface tension of MCH we use  $\sigma_{lg} = 22.72 \frac{\text{dyn}}{\text{cm}}$  for  $T = 30^\circ\text{C}$  [15]. Adjusting the geometry of the patterns to the experimental ones we calculate  $\Gamma_p$  and  $\Gamma_t$  as functions of  $\Delta T$ . We emphasize that at this stage there are no free parameters left in the model. The resulting curves



are shown in Fig. 4. For both quantities we obtain good quantitative agreement with the experimental results. In the filling regime ( $5K \lesssim \Delta T \lesssim 8K$ ) the calculated  $\Gamma_p(\Delta T)$  exhibits a power-law behavior  $\Gamma_p \propto \Delta T^{-\beta_p}$  with an effective exponent  $\beta_p \approx 2.4$ . The apparent disagreement with the value  $\beta_p \approx 0.76$  used in Ref. [4] can be explained by the mislocation of the filling regime on the experimental  $\Gamma_p(\Delta T)$  curve due to the large error bars for the data points at large  $\Delta T$ . The weak crossover at  $\Delta T \approx 8K$  corresponds to the disappearance of the interfacial meniscus, so that for larger values of  $\Delta T$  the interface follows the shape of the substrate. We have found that for larger cavities this crossover becomes more pronounced and for sufficiently large  $D$  and  $R$  we obtain the exponent  $\beta_p = 3.4$ .

In summary, as function of undersaturation we have studied complete wetting of four classes of substrates structured by one- and two-dimensional periodic patterns of fixed depth and we have identified four scaling regimes. The filling and the post-filling evolutions of the interfacial profiles do not depend on the periodicity of the patterns, but are determined by a single isolated cavity. For sufficiently deep structures there exists a range of undersaturations, in which the midpoint interfacial heights, obtained for different patterns, can be expressed in terms of a single scaling function. For small undersaturations, the single-cavity behavior crosses over to one dominated by the presence of many of them, for which the interfacial thickness increases as on a planar substrate, but characterized by an effective geometry-dependent Hamaker constant. Ultimately, for very small undersaturations the wetting film thickness becomes independent of the geometrical substrate structures.

- 
- [1] T. Yanagishita, K. Nishio, and H. Masuda, *Adv. Mater.* **17**, 2241 (2005).
  - [2] E. Martines, K. Seunarine, H. Morgan, N. Gadegaard, C. D. W. Wilkinson, and M. O. Riehle, *Nano Lett.* **5**, 2097 (2005).
  - [3] E. Delamarche, D. Junker, and H. Schmid, *Adv. Mater.* **17**, 2911 (2005); and references therein.
  - [4] O. Gang, K. J. Alvine, M. Fukuto, P. S. Pershan, C. T. Black, and B. M. Ocko, *Phys. Rev. Lett.* **95**, 217801 (2005).
  - [5] L. Bruschi, A. Carlin, and G. Mistura, *Phys. Rev. Lett.* **89**, 166101 (2002).
  - [6] C. Rascón and A. O. Parry, *Nature* **407**, 986 (2000); *J. Chem. Phys.* **112**, 5157 (2000).

- [7] A. O. Parry, M. J. Greenaal, and J. M. Romero-Enrique, Phys. Rev. Lett. **90**, 046101 (2003).
- [8] D. B. Abraham, A. O. Parry, and A. J. Wood, Europhys. Lett. **60**, 106 (2002).
- [9] C. Rascón and A. O. Parry, Phys. Rev. Lett. **94**, 096103 (2005).
- [10] A. B. D. Cassie, Diss. Faraday Soc. **3**, 11 (1948).
- [11] S. Dietrich, in *Phase Transitions and Critical Phenomena*, edited by C. Domb and J. L. Lebowitz (Academic, New York, 1988), vol. 12, p. 1.
- [12] G. A. Darbellay and J. M. Yeomans, J. Phys. A: Math. Gen. **25**, 4275 (1992).
- [13] M. O. Robbins, D. Andelman, and J. F. Joanny, Phys. Rev. A **43**, 4344 (1991).
- [14] S. Goldman, J. Phys. Chem. **80**, 1697 (1976).
- [15] J. J. Jasper, J. Phys. Chem. Ref. Data, **1**, 841 (1972).